THE JOURNAL OF BIOLOGICAL CHEMISTRY VOL. 286, NO. 47, pp. 40943–40953, November 25, 2011
Printed in the U.S.A.

Tyrosine Phosphorylation as a Conformational Switch

A CASE STUDY OF INTEGRIN β_3 CYTOPLASMIC TAIL[*][S]

Received for publication, February 17, 2011, and in revised form, August 26, 2011 Published, JBC Papers in Press, September 28, 2011, DOI 10.1074/jbc.M111.231951

Lalit Deshmukh[‡§], **Nahum Meller**[¶], **Nathan Alder**[‖], **Tatiana Byzova**[¶], **and Olga Vinogradova**[‡1]

From the Departments of [‡]Pharmaceutical Sciences, School of Pharmacy and [‖]Molecular and Cell Biology, University of Connecticut, Storrs, Connecticut 06269, the [¶]Department of Molecular Cardiology, Lerner Research Institute, Cleveland Clinic Foundation, Cleveland, Ohio 44195, and the [§]Laboratory of Chemical Physics, NIDDK, National Institutes of Health, Bethesda, Maryland 20892

Reversible protein phosphorylation is vital for many fundamental cellular processes. The actual impact of adding and removing phosphate group(s) is 3-fold: changes in the local/global geometry, alterations in the electrostatic potential and, as the result of both, modified protein-target interactions. Here we present a comprehensive structural investigation of the effects of phosphorylation on the conformational as well as functional states of a crucial cell surface receptor, $\alpha_{IIb}\beta_3$ integrin. We have analyzed phosphorylated (Tyr^{747} and Tyr^{759}) β_3 integrin cytoplasmic tail (CT) primarily by NMR, and our data demonstrate that under both aqueous and membrane-mimetic conditions, phosphorylation causes substantial conformational rearrangements. These changes originate from novel ionic interactions and revised phospholipid binding. Under aqueous conditions, the critical Tyr^{747} phosphorylation prevents β_3CT from binding to its heterodimer partner α_{IIb}CT, thus likely maintaining an activated state of the receptor. This conclusion was tested *in vivo* and confirmed by integrin-dependent endothelial cells adhesion assay. Under membrane-mimetic conditions, phosphorylation results in a modified membrane embedding characterized by significant changes in the secondary structure pattern and the overall fold of β_3CT. Collectively these data provide unique molecular insights into multiple regulatory roles of phosphorylation.

Protein phosphorylation, initially discovered in the mid 1950s (1), today is considered as one of the most crucial cell signaling events. It is a reversible, ubiquitous switch which regulates nearly every aspect of prokaryotic and eukaryotic cell life and has been linked to many pathogenic processes. Phosphorylation involves a covalent attachment of the negatively charged phosphate group to the side chains of serine (86.4%), threonine (11.8%), and tyrosine (1.8%) residues in eukaryotes (2), which may result in local and/or global conformational rearrangement or induce transitions from order to disorder and *vice versa* (3). Moreover, it may alter protein function by modifying its interactions with the substrates or by varying the equilibrium between different conformational states. A total comprehension of these transitions is crucial for enhancing our knowledge of the signal transduction processes.

Integrins, a major class of non-covalent heterodimeric glycoprotein cell surface receptors, have been chosen for investigating the effects of phosphorylation in present work. Integrins are among the most studied and best characterized cell adhesion molecules. Each integrin subunit contains a large extracellular ligand-binding portion, a single membrane-spanning domain, and a short cytoplasmic tail devoid of any enzymatic activity (4). The unique bidirectional flow of information through integrins involves inside-out signals, which allow them to interact with extracellular soluble ligands, and ligand-dependent outside-in signals, which trigger the cellular response to cell adhesion. The integrins extracellular matrix (ECM)[2] interactions are controlled by integrins extracellular domains, whereas integrins-cytoplasmic proteins interactions are controlled via their cytoplasmic tails (CTs). This integration of extracellular and intracellular compartments allows dynamic regulation of many cellular processes including cell migration, shape change, proliferation, and differentiation (5). Integrin regulated signaling pathways, which involve direct or indirect interaction of the integrin CTs with integrin-associated proteins, are often controlled through phosphorylation.

Although platelet integrin β_3CT includes several phosphorylation sites (two tyrosines, one serine and multiple threonines), only tyrosine phosphorylation is found to be specific for the outside-in signaling (6). However, despite the crucial role of tyrosine phosphorylation for β_3 integrin function, the structural details describing the consequences of this process remain unknown. In this study we have investigated the effects of tyrosine phosphorylation on β_3CT under both, aqueous and membrane-mimic, environments. Our data demonstrate that, in comparison to the non-phosphorylated form (7, 8), under aqueous conditions phosphorylation of Tyr^{747} and/or Tyr^{759} of β_3CT induces a novel fold which precludes α_{IIb}/β_3 complex formation, thereby preserving the activated state of the recep-

* This work was supported in part by American Heart Association and National Institutes of Health (NIH) Grants (to O. V.) and NIH grants (to T. B.).

[S] The on-line version of this article (available at http://www.jbc.org) contains supplemental Figs. S1–S7.

[1] To whom correspondence should be addressed: Dept. of Pharmaceutical Sciences, 69 North Eagleville Rd., Unit 3092, Storrs, CT 06269-3092. Tel.: 860-486-2972; Fax: 860-486-6857; E-mail: olga.vinogradova@uconn.edu.

[2] The abbreviations used are: ECM, extracellular matrix; Ab, antibody; β_3NP, non-phosphorylated β_3CT; CT, cytoplasmic tail; DPC, dodecyl-phosphocholine; DSA, doxyl stearic acid; FN, fibronectin; IPTG, isopropyl β-D-1-thiogalactopyranoside; KO, knock-out; K_{SV}, Stern-Volmer quenching constant; MS, mass spectrometry; NOESY, nuclear overhauser enhancement spectroscopy; NMR, nuclear magnetic resonance; HSQC, heteronuclear single quantum correlation; PRE, paramagnetic relaxation enhancement; RP-HPLC, reversed phase high pressure liquid chromatography; VN, vitronectin.

tor. In presence of dodecyl-phosphocholine (DPC) tyrosine(s) phosphorylation results in significant conformational rearrangements of β_3CT coupled to a considerable perturbation of its interaction with the membrane. Together, these data define a critical role of tyrosine phosphorylation, in general, in the regulation of signal transduction as well as in controlling β_3 integrin function.

EXPERIMENTAL PROCEDURES

Peptide Synthesis—Short tyrosine(s)-phosphorylated peptides corresponding to NMPβ_3 and BPβ_3Pep, (^{720}TIHDRKEFAKFEEERARAKWDTANNPLpYK^{748}) and (^{736}RAKWDTANNPLpYKEATSTFTNITpYRGT^{762}) respectively, were chemically synthesized (Genemed Synthesis, Inc.).

Expression and Purification—Cloning, expression, and purification of α_{IIb}CT, β_3CT (non-phosphorylated form hereafter referred to as β_3NP), and MBP-α_{IIb} have been described previously (7). To produce ^{15}N and/or ^{13}C isotopically labeled α_{IIb}CT and β_3CTs, cells were grown in M9 minimal medium containing $^{15}NH_4Cl$ (1.1 g/liter) and ^{13}C glucose (2.5 g/liter) as the sole source of nitrogen and carbon. Tyrosine phosphorylation of β_3CT (mono-phosphorylated at Tyr-^{747}, hereafter referred to as β_3MP, and bi-phosphorylated at Tyr^{747}and Tyr^{759}, hereafter referred to as β_3BP) has been achieved *in vivo* by using TKB1 bacterial cell line from Stratagene following the manufacturer's protocol for the recombinant protein induction. Single amino acid mutations were made by using the QuikChange site-directed mutagenesis kit (Stratagene).

Mass Spectroscopy—Mass spectral analyses were performed on a quadrupole time-of-flight (Q-TOF) mass spectrometer (QSTAR Elite) equipped with an ESI source. The data acquisition was under the control of the Analyst QS software (Foster City, CA). All samples were dissolved in methanol:water mixture to achieve final concentration of 40 μM. Samples were infused into the ESI source at a flow rate of 10 μl/min by using the built-in syringe pump. Typical source conditions for Q-STAR were as follows: capillary voltage (5500V), declustering potential (215V), resolution (15000, full width-half maximum).

Tryptophan Fluorescence Quenching—Steady-state fluorescence was measured with a SPEX Fluorolog FL3–22 spectrometer (Jobin Yvon, Edison, NJ) equipped with double-grating excitation and emission monochromators. Emission scans for Trp fluorescence (λ_{ex} = 295 nm; λ_{em} = 310 to 400 nm at 1-nm intervals with 2 nm and 4 nm excitation and emission bandpass, respectively) were performed using samples (20–37 μM protein, pH 5.9) in 4 × 4 mm quartz microcells. Iodide Trp quenching was measured by titrating two equivalent samples in parallel with aliquots from either 2.5 M KI or 2.5 M KCl stocks, each containing 5 mM $Na_2S_2O_3$. Maximum intensities from each KI titration point were corrected by the KCl-containing samples to account for dilution and ionic strength and analyzed according to the Stern-Volmer law: $(F_0/F) - 1 = K_{SV}[I^-]$ where F_0 and F are the net intensities in the absence and presence of I^-, respectively, and K_{SV} is the Stern-Volmer quenching constant. All experiments were repeated three times.

EC Transfection and Adhesion Assay—Lung EC at passage 2 were suspended at 5 × 10^6/ml in Optimem media with 10 μg/ml pCDNA3.1 (empty or expressing β_3 WT or mutants) and 2 μg/ml pMAX-GFP. 100-μl portions were transferred to nucleofection cuvettes and pulsed using amaxa Biosystems nucleofector, program M-003. The cells were plated in growth media on VN-coated dishes, and sodium butyrate (at 5 mM final concentration) was added. 96-well plates were coated 1 h at 37 °C with 0.1 μg/ml VN, blocked 1 h at 37 °C with 1% heat-denatured BSA in PBS and washed in 3× PBS. Transfected cells were harvested 72 h post-transfection by brief trypsinization, washed, and suspended in DMEM:F12 containing 0.2% BSA. 2 × 10^4 cells in 60 μl volume were plated per well and allowed to adhere for 25 min. The wells were washed 5× in DMEM:F12 and the cells fixed 10′ in 2% formaldehyde in PBS. GFP images at 5x magnification were acquired and composite images encompassing the entire wells were constructed. Amounts of GFP-positive cells per well were quantified using ImageJ software. Portion of the transfected cells were analyzed by FACS using $\alpha_v\beta_3$ antibodies to compare expression levels of the β_3 constructs.

NMR Spectroscopy—Chemical shift assignments of β_3CT have been determined previously (7) and have been modified to address the effects of phosphorylation and changes in pH values. All the NMR experiments were performed on Varian 600MHz and 800 MHz equipped with inverse-triple resonance cold-probes and were processed with NMRPipe (9) and analyzed by CCPN software suite (10). Earlier we have used aqueous conditions (pH 6.1) to understandthe $\alpha_{IIb}\beta_3$ heterodimer interface (7). However, because of the apparent solubility issues of phosphorylated constructs at pH 6.1, pH of the β_3MP samples was reduced to 5.9 to achieve sufficient concentrations for structure determination. Both β_3NP and β_3MP did not demonstrate substantial pH-dependent conformational differences judging by their chemical shift perturbation data (supplemental Fig. S4*A*).^{1}H-^{15}N HSQC titration experiments (Fig. 3, *C* and *D*) were performed in water at 25 °C at pH 6.1. Transferred NOESY experiments (Fig. 3, *E* and *F*) for different peptides were performed at 25 °C at pH 6.1. Different ratios of the peptides to the binding partner were investigated to find the optimal range for NOE transfer for each particular analysis. The resonance assignments of unlabeled peptides were made using conventional two-dimensional ^{1}H-^{1}H TOCSY and NOESY spectra (11) by CCPN software suite (10).

To characterize the structures and membrane-binding properties of phosphorylated β_3CTs, 0.07–0.9 mM ^{15}N- and/or ^{13}C-labeled β_3CTs (β_3NP, β_3MP and β_3BP) were dissolved in 60–300 mM deuterated DPC solution (Sigma-Aldrich) prepared in 20 mM sodium phosphate buffer, 5 mM Ca^{2+} at pH 5.9. The pH was monitored with pH strips (EMD Chemicals). All NMR experiments involving membrane-mimetic conditions were performed at 40 °C. To determine the location of different β_3 constructs relative to the micelle surface, steric acid compounds (16-DSA and 5-DSA) were used. Both were dissolved in 50 mM deuterated DPC solution to make 50 mM stock solution. These solutions were then added to the protein + DPC solution to achieve the following final ratios of protein: 5/16 DSA: DPC: 1:10:750 (β_3NP); 1:12:1000 (β_3MP); 1:14:1000 (β_3BP). The effects of the spin labels were observed by comparing the peak intensities (supplemental Fig. S6) in ^{1}H-^{15}N HSQC spectra. For

calculating the intensity ratios, the spectra were processed with 10 Hz exponential broadening in direct dimension and zero-filled to 2048 × 1024 data points in t2 and t1, respectively. For the NMR dynamics study of β_3NP, ^{1}H-^{15}N NOE, ^{15}N T_1, and T_2 data under aqueous (25 °C) and membrane mimetic conditions (40 °C) were collected on a Varian Inova 600 MHz spectrometer. ^{15}N T_1 values were measured from the spectra recorded with 8 different durations of the delay: T = 30, 90, 150, 250, 400, 600, 800, 1200 ms. ^{15}N T_2 values were determined from spectra recorded with 8 different durations of the delay: T = 10, 20, 30, 50, 70, 90, 110, 150 ms. Steady-state hetero-nuclear ^{1}H-^{15}N NOE values were determined from spectra recorded with 5 s relaxation delay and the presence and absence of a proton presaturation period of 5 s. T_1, T_2, and NOE values were extracted by a curve-fitting subroutine included in the CCPN software suite (10) (supplemental Fig. S7). The rotational correlation time (τ_c) values were estimated to be ~5 ns in aqueous solution and 9 nanoseconds in DPC using TENSOR-2 (32) indicating the differences in overall tumbling associated with micelles binding.

Structure Calculation—Table 1 lists detailed structural statistics of the final fifteen lowest energy conformers of β_3NP, β_3MP, and β_3BP under aqueous and membrane-mimetic conditions along with the two-dimensional and three-dimensional NMR experiments utilized for individual structure determination. For β_3MP and β_3BP in presence of DPC micelles, the backbone, ψ and ϕ, dihedral angle restraints were obtained by using Talos+ (12). All the initial structure calculations were performed using CYANA 2.1 (13). Hydrogen bond restraints (in the case of β_3MP under aqueous conditions) were introduced during the final stages of calculations. Sixty lowest energy structures from CYANA were subjected to molecular dynamics simulations in explicit water (14) using CNS (15). For β_3NP under membrane-mimetic conditions, sixty structures were calculated by utilizing previously (8) determined NOE and dihedral restraints with the help of CYANA and later were refined in explicit water to maintain consistency and for a more accurate comparison. None of the structures have NOE and dihedral angle violations more than 0.5 Å and 5°, respectively. The Protein Structure Software suite (PSVS; courtesy of CABM Structural Bioinformatics Laboratory, Rutgers State University of New Jersey) was used for structure quality assessment and validation.

RESULTS

Preparation of Tyrosine-phosphorylated Integrin β_3 Cytoplasmic Tail for Structural Analysis—Phosphorylation has long been considered as a critical regulatory apparatus in signal transduction and nuclear magnetic resonance (NMR) spectroscopy is a pertinent technique for deciphering the emanating conformational changes imparted by phosphorylation. However, the first step in investigation of phosphorylation by NMR, production of the phosphorylated, isotopically labeled proteins in adequate amounts, is usually an uphill task. In the case of β_3CT (see supplemental Fig. S1 for sequence details), the TKB1 bacterial cell line (Stratagene), carrying Elk tyrosine kinase gene controlled by the *trp* promoter, was found to yield sufficient quantities of (tyrosine)-phosphorylated protein. Although it has been suggested that this *in vivo* approach is not as efficient as the *in vitro* technique due to the deleterious effects of Elk tyrosine kinase on the bacteria (16), we could produce reasonable amounts of phosphorylated β_3 by using unusually short induction times (IPTG induction of β_3 at A_{600} ~0.3 followed in 2 h by tryptophan induction of Elk). Supplemental Fig. S2 (SM) depicts the reversed phase, RP-HPLC chromatogram of β_3CT expressed in TKB1 cells and the deconvoluted mass spectra of the three HPLC peaks. The MS analysis reveals that the peaks eluting at 23, 24, and 26% of acetonitrile gradient correspond to the bi-phosphorylated, mono-phosphorylated, and non-phosphorylated β_3CT, respectively. Our initial assumption was that we will achieve almost equal populations of the two mono-phosphorylated β_3CT constructs (pY^{747} and pY^{759} respectively) which would be very difficult to separate. However, a closer inspection of superimposed ^{1}H-^{15}N HSQC spectra of these three HPLC peaks, Fig. 1*A* and supplemental Fig. S3*A*, demonstrates that the middle peak in the chromatogram is pY^{747}-β_3CT and does not contain any pY^{759}-β_3CT. Though Elk is known to be a promiscuous tyrosine kinase, the efficiency of phosphorylation in β_3CT appeared to be very different for the two tyrosine residues (Tyr^{747}, Tyr^{759}). While we could produce NMR quantities of pY^{747}-β_3CT (hereafter referred to as β_3MP) and extremely limited quantities of pY^{747}, pY^{759}-β_3CT (hereafter referred to as β_3BP); we could not generate any pY^{759}-β_3CT. One possible explanation for the lack of pY^{759} product may be the flexibility and dynamic nature of the β_3CT's C terminus in the absence of pY^{747}. To substantiate this hypothesis, we introduced conservative point Y747F or Y759F mutations in β_3CT construct by using site-directed mutagenesis (QuikChange). Supplemental Fig. S3*B* depicts the superimposition of ^{1}H-^{15}N HSQC spectra of these mutants with the wild type β_3CT. Expression of these mutants in TKB1 cells confirmed our observation. As in the case of their wild type counterparts, we could produce pY^{747} for Y759F mutant (supplemental Fig. S3*C*), but were unable to phosphorylate the Y747F mutant.

Phosphorylation of Tyr^{747} Results in Structural Rearrangement of β_3CT under Aqueous Conditions—The superimposition of ^{1}H-^{15}N-HSQC spectra for β_3NP, β_3MP and β_3BP under aqueous conditions is shown in Fig. 1*A* and the subsequent chemical shift perturbations are presented in Fig. 1*C*. From these data, it is clear that phosphorylation not only affects the nearby residues (^{743}NN-LpYKEA^{750} and ^{757}ITpYRGT^{762}) but also influences the membrane-proximal region (K^{716}-D^{723}). These latter chemical shift perturbations are common to both, β_3MP and β_3BP constructs, suggesting an intramolecular interaction between the membrane-proximal and ^{744}NPLpY^{747} regions. This interaction is a direct result of Tyr^{747} phosphorylation, most probably due to a formation of the salt bridge between the negatively charged phosphate group and the positively charged/polar side-chain(s) of the N-terminal amino acid(s). To better understand this change, we acquired ^{1}H-^{1}H two dimensional (2D) Nuclear Overhauser Enhancement Spectroscopy (NOESY) and three-dimensional ^{15}N-edited NOESY spectra of β_3MP, which allowed us to structurally characterize β_3MP under aqueous conditions. The overall fold of β_3MP is shown in Fig. 2, *A* and *B* (PDB ID: 2ljf, see statistics in Table 1). Interestingly, the negatively charged phosphate group of pY^{747}

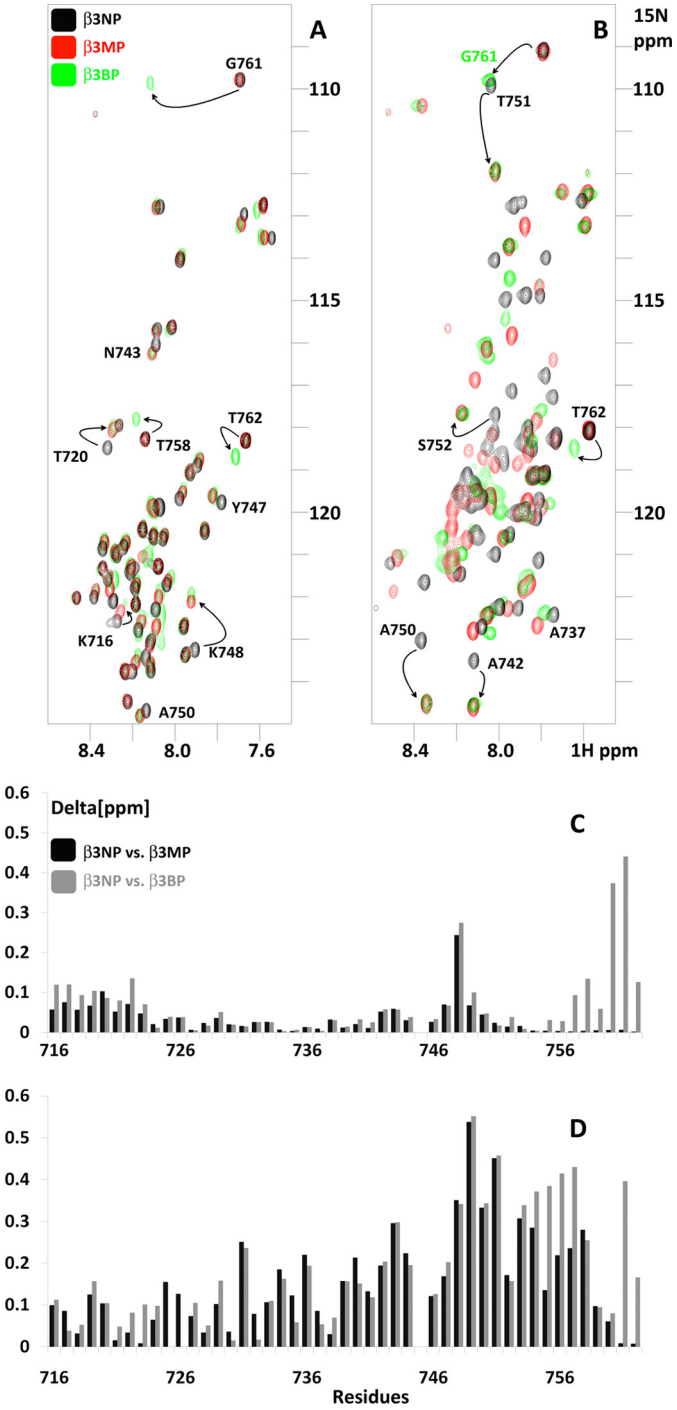

FIGURE 1. **Tyrosine(s) phosphorylation of β_3CT.** ^{1}H-^{15}N HSQC spectra of ^{15}N-labeled β_3NP (*black*), β_3MP (*red*), and β_3BP (lime): (*A*) in aqueous solution, pH 6.1, 25 °C; (*B*) in DPC micelles, pH 5.9, 40 °C. Some critical residues undergoing conformational change are labeled and marked with *arrows*. Chemical shift changes of β_3 tails due to tyrosine phosphorylation: (*C*) in aqueous solution, pH 6.1, 25 °C; (*D*) in DPC micelles, pH 5.9, 40 °C. Delta [ppm] refers to the combined HN and N chemical shift changes according to the equation: $\Delta\delta(HN,N) = ((\Delta\delta_{HN}^2 + 0.2(\Delta\delta_N)^2)^{1/2}$, where $\Delta\delta = \delta_{bound} - \delta_{free}$. Bars are colored as follows: β_3NP *versus* β_3MP (*dark gray*) and β_3NP *versus* β_3BP (*light gray*)

creates a salt-bridge with the positively charged side-chain of Lys^{738}, which, in turn, affects the orientation of Trp^{739} indole side chain. This bulky, hydrophobic side chain forges contacts with the methyl groups of membrane-proximal residues (Leu^{717} is shown as an example, Fig. 2*B*) and the resulting compact conformation is then further stabilized by hydrogen bond between the side-chains of D^{740}-N^{743}. The first turn of the membrane-proximal helix, found in the $\alpha_{IIb}\beta_3$ heterodimer (7), is not formed in β_3MP and the helical region spans only from Lys^{725} to Lys^{729}. The C-terminal region (F^{754}-T^{762}) is dynamically unstructured. Interaction of Trp^{739} with the membrane-proximal residues supports the notion that it could be situated near, but not necessarily within, the membrane. This is consistent with our prior findings that both Trp^{739} and Tyr^{747} can interact with phospholipids (8). Compared with the compact conformation of β_3MP, β_3NP is much more dynamic and largely unstructured, as has been reported previously (7, 17), except for a reverse turn formed around the ^{744}NPLY^{747} motif and helical tendencies in the membrane proximal region (Fig. 2, *E* and *F*, statistics of the ensemble are presented in Table 1). Moreover, the dynamic nature of β_3NP under aqueous conditions is supported by NMR relaxation measurements as most of the HetNOE values are below 0.3 (supplemental Fig. S7, *A–D*). Sequential connectivity maps for both ensembles are provided (supplemental Fig. S5).

It is imperative to mention that in the case of β_3MP, although the chemical shift changes due to pY^{747} are very modest and absolute chemical shift values are close to the random coil values, we were able to observe long-range NOEs. In dynamic systems where the folded, transient, and unstructured conformers are in fast exchange, the observed NOEs can be averaged over multiple conformers, and not all the contacts are satisfied by a single conformer. Any attempt to fulfill all such NOE contacts simultaneously might lead to an over-constrained system. Hence, to independently confirm this novel compact conformation of β_3MP is not artificial, we performed iodide quenching of tryptophan fluorescence to determine the relative exposure of W^{739} indole side chain of β_3MP and β_3NP to the aqueous environment (Fig. 2*C*). The measured K_{SV} values were lower for β_3MP ($K_{SV} = 3.09 \pm 0.43\ M^{-1}$) than for β_3NP ($K_{SV} = 4.35 \pm 0.56\ M^{-1}$). Our steady-state emission scans strongly suggest that the higher K_{SV} values of the β_3NP are not due to the higher unquenched fluorescence lifetime because the specific fluorescence intensities and λ_{max} values are equivalent for both proteins. This indicates that Trp^{739} in β_3MP is indeed better shielded from solvent exposure than its non-phosphorylated counterpart by virtue of its compact fold and due to the hydrophobic interactions with the N-terminal residues. In addition, we investigated the importance of pY^{747}-K^{738} salt bridge by using NMR salt titrations. The rationale behind these experiments was that the electrostatic interactions responsible for the β_3MP fold should be affected by changes in salt concentrations. Supplemental Fig. S4*B* displays the distribution of chemical shifts for β_3MP under the different ionic strength buffers. High salt concentration, indeed, has a major impact on the changes in chemical shifts resulting in significant decline of chemical shift perturbations throughout the membrane proximal region of β_3CT.

To further validate and test the biological significance of this fold, we performed site-directed mutagenesis, point mutation K738E (Quikchange) (see supplemental Fig. S1 for sequence details) and investigated both *in vitro* and *in vivo* properties of

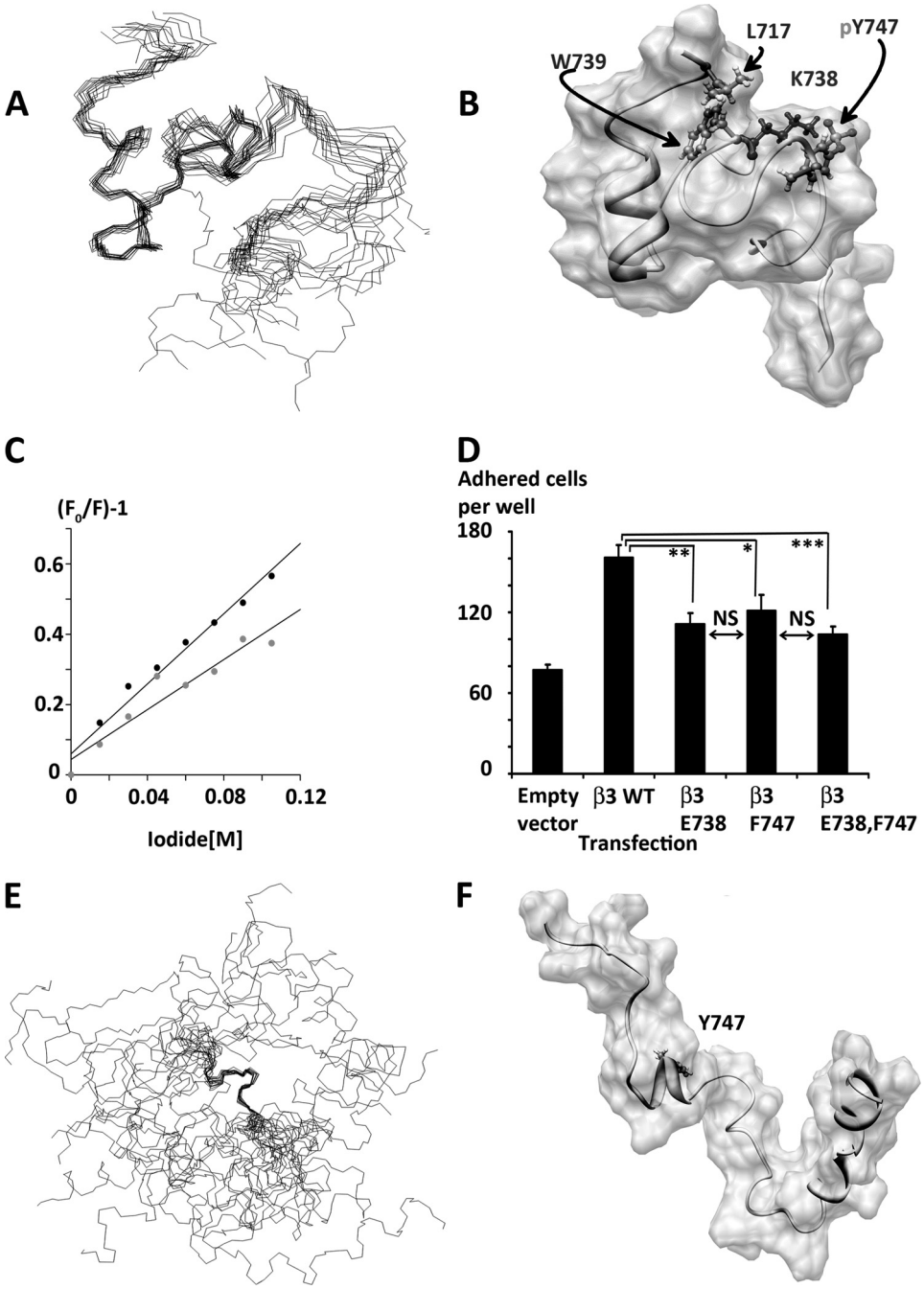

FIGURE 2. **Structures of β_3NP and β_3MP under aqueous conditions.** Molecular graphics images were produced by using the UCSF Chimera package (29). *A*, backbone superimposition on fifteen lowest energy conformers of β_3MP. Residues ^{722}H-D^{740} are superimposed; *B*, *ribbon diagram* of a conformer closest to the mean with the same view. Surface is shown in *gray*. Some of the crucial residues are shown in *ball and stick representation*. Positively charged residues are shown in *blue*; negatively charged in *red*; hydrophobic residues in *gray*; *C*, representative Stern-Volmer plots for β_3NP (in *black*, mean Ksv is 4.35 $\pm$ 0.56) and β_3MP (in *red*, mean Ksv is 3.09 $\pm$ 0.43); *D*, mutation of either Phe^{747} or Lys^{738} inhibits EC adhesion to VN. Lung EC isolated from β_3 KO mice were co-transfected with pmax-GFP and either pCDNA3.1 (Empty vector) or pCDNA3.1 β_3WT, K738E, Y747F, or K738E/Y747F. 72 h post-transfection cells were collected, plated in VN-coated 96 wells for 25 min, washed five times, and fixed. The wells were photographed and GFP-positive cells were counted. Similar expression levels of β_3 in the different transfections were confirmed by FACS stain for $\alpha_v\beta_3$ (not shown). Statistical analysis is presented as mean $\pm$ S.E., *, $p < 0.05$; **, $p < 0.01$; ***, $p < 0.001$ Students *t* test. *E*, backbone superimposition on fifteen lowest energy conformers of β_3NP. The ^{744}NPLYK^{748} motif is superimposed; *F*, *ribbon diagram* of a conformer. Surface is shown in *gray*.

this mutant. Residue Lys^{738} was selected for this analysis as it plays a critical role in the conformation change of β_3MP and as per our knowledge has not been implicated in any interactions with known integrin modulators, such as talins or kindlins. Hence the effect of this mutation on integrin activation state should be attributed to the structural integrity rather than external factors. Theoretically, this K738E charge reversal should abolish the salt-bridge in β_3MP, making the conformational change due to Tyr^{747} phosphorylation challenging. As expected, the chemical shift perturbations in the membrane proximal region due to Tyr^{747} phosphorylation are smaller than its wild type (WT) counterpart and are randomly distributed

TABLE 1
Structural statistics of phosphorylated and non-phosphorylated β_3 constructs under aqueous and membrane-mimetic conditions

	β_3NP (water)	β_3MP (water)	β_3NP (DPC)	β_3MP (DPC)	β_3BP (DPC)
Distance restraints					
All	797	798	925	603	505
Short range (i-j < = 1)	482	293	703	436	374
Medium-range (1< i-j <5)	314	440	202	147	121
Long-range (i-j > = 5)	1	65	20	20	10
Ambiguous	7	10	NA	NA	NA
Dihedral Angle restraints[a]					
Phi (ϕ)	NA	NA	33	28	29
Psi (ψ)	NA	NA	32	28	29
Hydrogen bond restraints[b]	NA	2	NA	NA	NA
Average CYANA target function value	2.80	3.71	2.54	1.42	0.77
Violations					
NOE	0.0318 ± 0.0015	0.0329 ± 0.0013	0.0261 ± 0.0014	0.0261 ± 0.0012	0.0260 ± 0.0016
cdih	NA	NA	0.5681 ± 0.1245	0.7094 ± 0.1551	0.9904 ± 0.1418
RMSD[c]					
Average backbone RMSD to mean	2.08 ± 0.75 Å	0.75 ± 0.20 Å	0.97 ± 0.35 Å	0.89 ± 0.31 Å	1.08 ± 0.37 Å
Average heavy atom RMSD to mean	3.18 ± 1.05 Å	1.34 ± 0.24 Å	1.66 ± 0.33 Å	1.77 ± 0.35 Å	1.90 ± 0.43 Å
VanderWaal Energy (kcal mol^{-1})[d]	−394.26 ± 8.52	−399.48±33.17	−414.26 ± 15.52	−373.72 ± 27.84	−367.34 ± 27.40
Deviation from idealized geometry					
Bonds(Å)	0.0134 ± 0.00056	0.0145 ± 0.00020	0.0118 ± 0.00025	0.0122 ± 0.00028	0.0122 ± 0.00040
Angles (°)	1.3771 ± 0.0363	1.4163 ± 0.0449	1.2298 ± 0.0179	1.1855 ± 0.0307	1.0897 ± 0.0418
Impropers (°)	1.2315 ± 0.1380	1.5317 ± 0.1282	1.3133 ± 0.1096	1.2279 ± 0.0947	1.1990 ± 0.0947
Ramchandran statistics[e]					
Residues in most favored regions	72.6%	49.3%	85.4%	78.3%	82.2%
Residues in additional allowed regions	23.6%	46.5%	9.9%	18.3%	16.6%
Residues in generously allowed regions	1.7%	3.9%	2.8%	3.4%	1.1%
Residues in disallowed regions	2.2%	0.3%	1.9%	0%	0.2%
NMR experiments	2D ^{1}H-^{1}H NOESY[f]	2D ^{1}H-^{1}H NOESY[f] 3D ^{15}N-edited NOESY[g]	Based on Ref. 8	3D ^{15}N-edited NOESY[h] 3D ^{13}C-edited NOESY[h] 3D ^{13}C-edited aromatic NOESY[h] 3D HNCO 3D HNCACB	3D ^{15}N-edited NOESY[h] 3D HNCO

[a] Generated from Talos+ (12).
[b] Hydrogen bonds were introduced in the last stage of structure calculations.
[c] The following residues are considered for the rmsd calculations: I) β_3NP(water): residues 720–735 II) β_3MP(water): residues 720–745 III) β_3NP(DPC): residues 722–745 IV) β_3MP(DPC): residues 720–745 V) β_3BP(DPC): residues 720–745.
[d] After refinement in explicit water by using CNS(15).
[e] All residues, calculated using the Protein Structure Software suite.
[f] 400 ms mixing time.
[g] 300 ms mixing time.
[h] 150 ms mixing time.

throughout the sequence with the major local effect shifted in C-terminal direction (supplemental Fig. S4*C*). Thus it can be argued that under *in vitro* conditions pY^{747}-K738E mutant probably exhibits behavior similar to that of β_3NP. The effect of this charge reversal was next tested in β_3 integrin-dependent endothelial cell (EC) adhesion to vitronectin (VN). EC isolated from β_3 knock-out (KO) mice were transfected with expression vectors for either WTβ_3 or substitution mutants Y747F, K738E, Y747F-K738E (see supplemental Fig. S1 for sequence details). As shown in Fig. 2*D*, expression of both K738E and Y747F mutants showed decreased adhesive response as compared with WT β_3 integrin expressing cells. Importantly, adhesion of K738E-expressing cells was similar to that of Y747F mutant and no further inhibition was observed in double K738E/Y747F mutant cells. As an additional control, K738E mutation was tested to find out whether it can reduce integrin ability to undergo activation, for example by preventing its interactions with talins or kidlins. As expected, this mutation did not result in diminished soluble fibrinogen binding mediated by $\alpha_{IIb}\beta_3$ integrin (supplemental Fig. S4*D*). Thus, the resulting differences in the activation states between this mutant and the wild type are related to the internal structural integrity. Combined, these data confirm the critical role of K^{738}/Y^{747} for the regulation of integrin-mediated cell adhesion and biological significance of novel β_3MP conformation.

Because of the challenges with sample preparation, we could not investigate structural details of β_3BP under aqueous conditions, but considering the similarity of chemical shifts of N-terminal residues between β_3MP and BP (Fig. 1, *A* and *C*) and the dynamic nature of the C terminus, it is safe to suggest that β_3BP accommodates a conformation similar to β_3MP and is distinct from β_3NP. Together these data indicate that upon phosphorylation β_3CT undergoes a substantial structural change, leading to a more compact conformation, which, in turn, might affect interactions between the receptor and intracellular adaptors.

Tyrosine Phosphorylation Preserves the Activated State of Integrin by Preventing the Interaction between β_3 and α_{IIb} Cytoplasmic Tails—In a previous study (7), we have structurally characterized the cytoplasmic domain of $\alpha_{IIb}\beta_3$ heterodimer. Our data revealed the underlying mechanism by which the inter-subunit clasp, R^{995}(α_{IIb}CT)-D^{723}(β_3CT) along with several other electrostatic and hydrophobic contacts (Fig. 3*A*), maintains the integrin in a resting state. Termination of these interactions eventually results in integrin activation. As tyrosine phosphorylation leads to a conformational rearrangement of β_3CT, we were curious to find out whether these changes

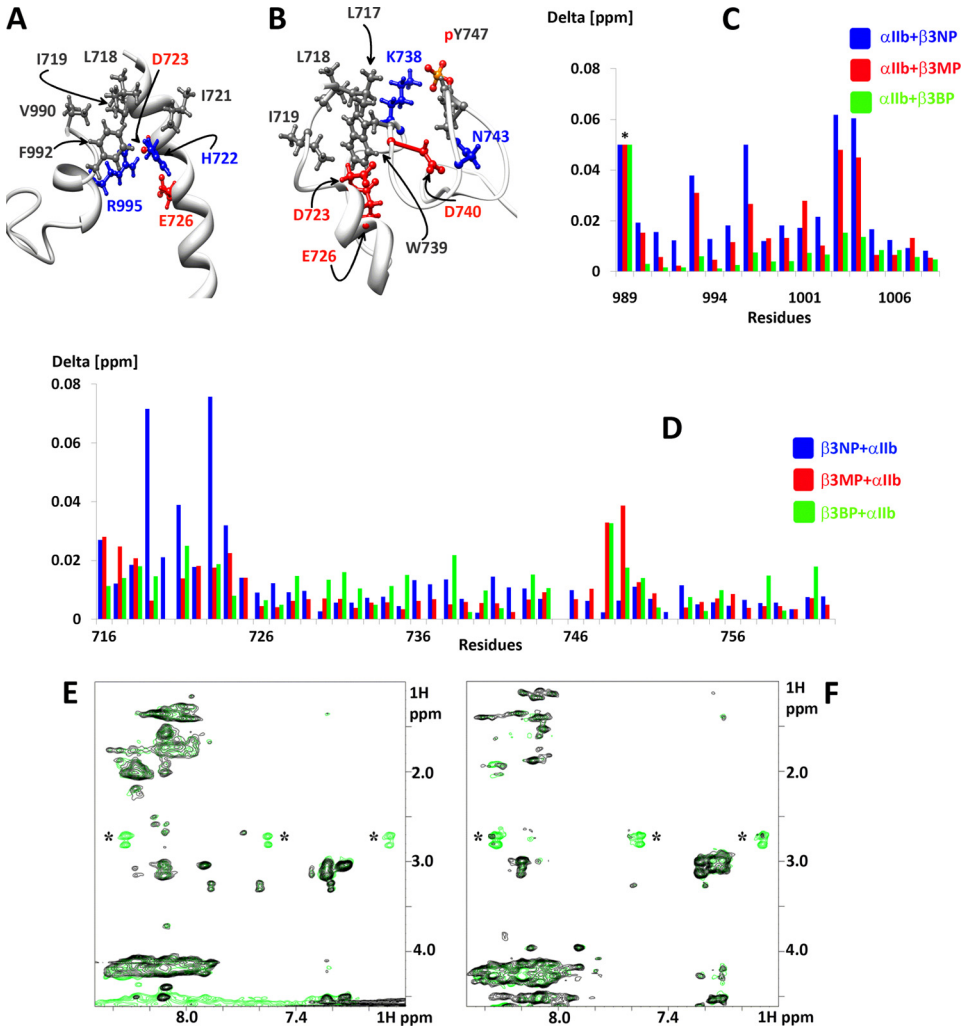

FIGURE 3. **Summary of α_{IIb}-β_3NP/MP/BP interactions.** *A*, expanded view of $\alpha_{IIb}\beta_3$ heterodimer membrane proximal interface; *B*, membrane proximal region of β_3MP; positively charged residues are shown in *blue*; negatively charged in *red*; hydrophobic residues in *gray*; *C*, chemical shift perturbations of ^{15}N-labeled α_{IIb} in presence of β_3NP (*blue*); β_3MP (*red*); β_3BP (*lime*), ^{989}K (marked with *) shows line broadening; *D*, chemical shift perturbations of ^{15}N-labeled β_3NP (*blue*); β_3MP (*red*); β_3BP (*lime*) in presence of α_{IIb}. Transferred NOESY experiments indicating the lack of α_{IIb}-β_3MP/BP interactions; *E*, superimposition of NOESY spectra for NMPβ_3 in absence(*black*) and presence (*lime*) of MBP-α_{IIb} at the ratio 20:1; *F*, superimposition of NOESY spectra for BPβ_3Pepin absence (*black*) and presence (*lime*) of MBP-α_{IIb} at the ratio 20:1. Peaks marked with * represent peaks from MBP-tag. All the transferred NOESY experiments were performed at 25 °C (400 ms mixing time) in 0.25× PBS buffer in presence of 6 mM $CaCl_2$ to stabilize α_{IIb} as described earlier (Vinogradova *et al.*, 25).

affect the formation of $\alpha_{IIb}\beta_3$ heterodimer. Superimposition of β_3MP structure with $\alpha_{IIb}\beta_3$ heterodimer revealed a steric clash between β_3MP and the α_{IIb} subunit indicating the possible difficulties in clasp formation (Figs. 3*B* and 5*A*). To test this prediction, we performed chemical shift mapping experiments similar to those done before to define $\alpha_{IIb}\beta_3$ cytoplasmic clasp (7). Non-labeled β_3NP, β_3MP, and β_3BP were titrated with ^{15}N-labeled α_{IIb}CT and the associated chemical shift perturbations were monitored. Chemical shift changes plotted as a function of residue numbers in α_{IIb}CT (Fig. 3*C*) indicate a gradual decrease upon β_3CT phosphorylation. These observations were also supported by the opposite experiments, where non-labeled α_{IIb}CT is titrated into solutions of ^{15}N-labeled β_3NP, β_3MP, and β_3BP. Fig. 3*D* shows the subsequent chemical shift changes plotted as a function of the residue number in β_3CT. It is important to mention that residues Lys^{748} and Glu^{749} are more perturbed in β_3MP than in β_3NP. This could indicate either the appearance of a new binding site, or an internal conformational rearrangement in β_3 tail. To examine the possibility of interaction between α_{IIb}CT and residues Lys^{748} and Glu^{749} of β_3CT, we utilized the transferred NOE (trNOE) method (18). This approach is well suited for characterization of such weak interactions and has been used in the elucidation of $\alpha_{IIb}\beta_3$ structure (7). The method detects appearance of additional peaks in the ligand's NOESY spectra upon its interaction with the target protein (19). α_{IIb}CT was fused to maltose-binding protein (MBP) tag to increase the molecular weight as higher molecular weight allows more favorable NOE transfer, the effect proven experimentally even despite of some independent local α_{IIb}CT motion (7). Because the full-length β_3 tail has limited solubility (20), we have used shorter β_3 peptides, NMPβ_3 containing the N-terminal residues, including pY^{747} and BPβ_3Pep containing the C-terminal residues, including both pY^{747} and pY^{759} (see supplemental Fig. S1, SM, for sequence details). No additional peaks were detected in NOESY spectra of these peptides upon addition of MBP-α_{IIb} under any of the conditions tested (Fig. 3, *E* and *F*). Thus based on all these data, it can be concluded that the chemical shift perturbations observed for residues Lys^{748}

and Glu[749] are due to an internal structural rearrangement. And tyrosine phosphorylation of β_3CT, indeed, prevents β_3 from making and/or maintaining contacts with α_{IIb}CT, thereby preserving the activated state of the receptor.

Phosphorylation Affects β_3CT Interaction with the Membrane—To address the effects of tyrosine(s) phosphorylation on β_3CT's interaction with lipid bilayer, we next investigated β_3MP and β_3BP in DPC detergent micelles. DPC has been used extensively as a membrane mimetic for NMR studies and was previously utilized to structurally characterize β_3NP (8) and other similar constructs (21, 22). In the presence of DPC micelles, β_3NP exhibits much more structured conformation even without its binding partner α_{IIb}CT (8). Moreover, we have demonstrated that several residues of β_3NP (Trp[739], Thr[741], Ala[742], Pro[745], and Tyr[747]) could interact with DPC micelles and these interactions initiate the formation of a second short α-helical region (Leu[746]-Asn[756]), which is not generally observed in either aqueous β_3 or $\alpha_{IIb}\beta_3$ heterodimer. These conclusions are also corroborated by the NMR relaxation measurements (supplemental Fig. S7, *E–H*). The whole β_3NP is tumbling along with the micelles except the last three C-terminal residues (RGT[763]) which are undergoing a significant local motion. However, both β_3MP and β_3BP behaved very differently as compared with β_3NP in DPC micelles. The superimposition of ^{1}H-^{15}N-HSQC spectra of β_3NP/MP/BP in DPC is depicted in Fig. 1*B* and the resultant chemical shift perturbations are presented in Fig. 1*D*. The shift differences between non-phosphorylated and phosphorylated constructs are quite significant (Fig. 1*D*). This may be due to the alterations in secondary structural elements because of the distinctive β_3-membrane interaction. Interestingly, the chemical shifts are almost identical for the affected mid-region (residues E[731]-T[753]) in β_3MP and β_3BP cases, indicating the likeness of the conformations in membrane environment. For β_3BP, as expected, the additional shift changes were associated with the second phosphorylation site (the C terminus residues, F[754]-T[762]) highlighting the possible differences from β_3MP. To confirm these hypotheses, we have performed a full scale NMR structural investigation of β_3MP (and partially for β_3BP) in DPC micelles. We have also tested the interactions of all three constructs (β_3NP/MP/BP) with the DPC micelles using the Paramagnetic Relaxation Enhancement (PRE) approach (23).

The overall folds of β_3NP, β_3MP and β_3BP are shown in Fig. 4, *A*, *C*, and *E*, respectively (PDB IDs: 2ljd and 2lje for β_3MP and β_3BP, respectively. The statistics are shown in Table 1; see under "Experimental Procedures" for additional details. Sequential connectivity maps are provided in supplemental Fig. S5). The prominent structural features of β_3NP in presence of DPC micelles, a membrane-proximal α-helix (K[716]-R[734]) followed by a flexible loop and another short helix (Y[747]-T[755]) (8), are extensively modified due to tyrosine phosphorylation. The membrane-proximal α-helix is slightly longer (K[716]-K[738]), however the C-terminal region directly following pY[747] is no longer helical except for some helical tendencies in A[750]-T[753] region. Another surprising finding is that the kink at residues D[723]/R[724] in β_3NP, which allows the helix to bend, bringing the flexible loop (K[738]-A[742]) into possible contact with the membrane surface, has shifted toward the residues K[725]/E[726] in β_3MP and β_3BP. The angles between the two portions of the

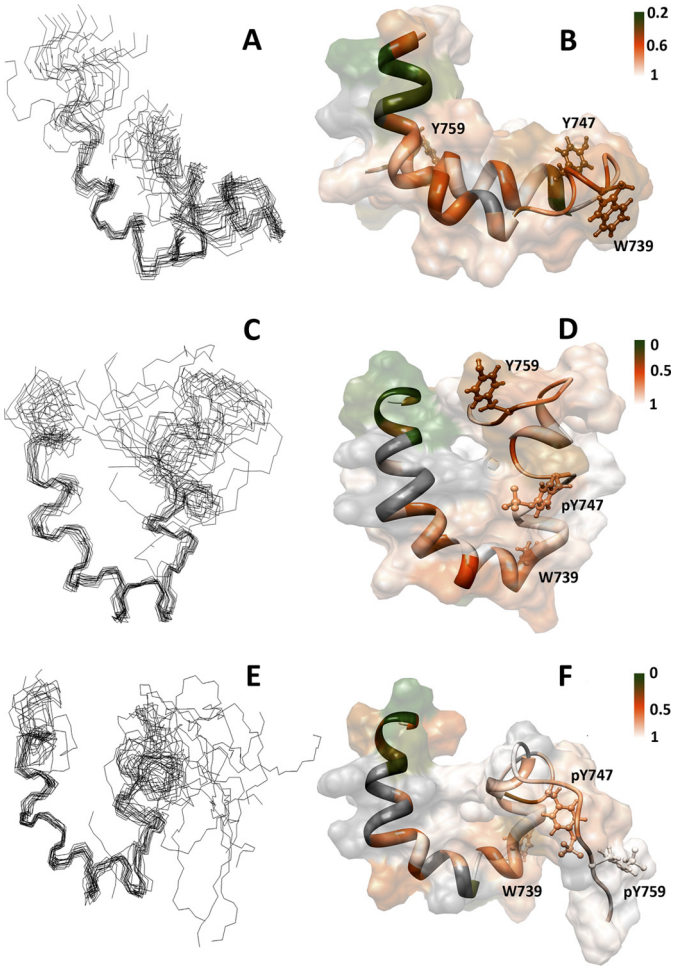

FIGURE 4. **Structures of β_3NP, β_3MP, and β_3BP in DPC micelles.** Molecular graphics images were produced by using the UCSF Chimera package (29). *A*, *C*, *E*, backbone superimposition on fifteen lowest energy conformers of β_3NP, β_3MP, β_3BP, respectively; *B*, *D*, *F*, *ribbon* representation of β_3NP, β_3MP, β_3NBP conformers closest to the mean structures. The intensity ratios from the PRE experiments (β_3NP/MP/BP+16-DSA+DPC) are mapped onto the surfaces of β_3NP, β_3MP, and β_3BP respectively. *Green to orange to white* color gradient is used to map the PRE intensities (respective color keys are shown adjacent to the figure). Overlapping residues, residues with missing information, and prolines are marked in *gray*.

membrane-proximal helices are not very well defined in all three structures. The recent structural study (21) of the non-phosphorylated $\beta_3$construct, where several additional N-terminal transmembrane residues of β_3 were cross-linked with α_{IIb} subunit, has reported that the residue Arg[724] of β_3CT formed a single-residue hinge and the angle between the two parts of the membrane proximal helix, defined based upon intramolecular NOEs between residues Phe[727] and Ile[721], is about 100°. We however, could not find evidence of the above mentioned NOEs in any of our NOESY experiments. The biological significance of mutual orientation of these two portions of the membrane-proximal helices requires further investigation as it could easily reflect the consequences of higher surface curvature of the micelles, in comparison with mostly flat lipid bilayer.

For β_3BP in the presence of DPC micelles, the lack of distance restraints (single three-dimensional ^{15}N-edited NOESY-HSQC experiment) resulted in inadequate structural convergence. Because of the challenges in preparation of ^{13}C,^{15}N-labeled

β_3BP we could not perform 3D ^{13}C -edited NOESY-HSQC experiment. To circumvent this issue, since the chemical shifts for the N-terminal residues (K^{716}-A^{750}) between β_3MP and β_3BP were virtually identical (Fig. 1, *B* and *D*), we introduced the additional distance restraints corresponding to these N-terminal amino acids from β_3MP in β_3BP structure calculations. These additional restraints have resolved the issue of convergence. As expected, the structure is very similar to β_3MP except a slightly sharper kink in membrane proximal helix and the orientation of C terminus residues (^{752}S-G^{762}). The crucial differences in C terminus arise due to the phosphorylation of Tyr^{759}, which probably affects the orientation of the ^{756}NITYR^{760} motif. In contrast to β_3MP, where Tyr^{759} interacts with the membrane (for more details, see below), in the case of β_3BP, pY^{759} is pointing in opposite direction away from the membrane due to the repulsion between the negatively charged phosphate groups of pY^{759} and DPC.

To determine how tyrosine(s) phosphorylation alters the membrane binding, we utilized the PRE approach. Two paramagnetic relaxation agents which selectively partition in hydrophobic environment, 5-doxyl stearic acid (5-DSA) and 16-DSA, (24) were introduced into the DPC micelles and the consequent drop in the intensities of the amide peaks of all three β_3 constructs was monitored. The doxyl moiety in 16-DSA is attached to the very end of the aliphatic chain and thus gets localized at the center of DPC micelles. In 5-DSA, on the other hand, the doxyl moiety is situated close to the polar head group and the membrane-water interface. Both these tags were utilized to determine the membrane-embedded residues. Supplemental Fig. S6 represents the intensity ratios of the backbone amide groups of β_3NP/MP/BP upon titration with 5-DSA and 16-DSA and Fig. 4, *B*, *D*, and *F* depict these ratios (selected for 16-DSA) mapped on the surfaces of β_3NP/MP/BP structures representing the direct contacts with the micelles. In the case of β_3NP, we confirmed some of our earlier intermolecular NOEs findings (8). The membrane-proximal residues (L^{717}-I^{721}) and Tyr^{747} of β_3NP are, indeed, inserted into the membrane. Moreover, the region ^{738}KWD^{740} is associated with the membrane surface judging by the drop in intensity ratios upon titration with 5-DSA, but not with 16-DSA (supplemental Fig. S6, *A* and *B*). Surprisingly, the C-terminal ^{756}NITYR^{760} motif of β_3NP also shows significant drop in peaks intensities in both cases (5-DSA and 16-DSA) and is probably associated with the membrane. Previously we could not detect any intermolecular NOEs to support this finding, which is due to the highly dynamic nature of this C-terminal region as confirmed by ^{15}N relaxation data (supplemental Fig. S7). Although the intensity ratios are rather similar for all β_3 constructs, we do see specific differences in the patterns of membrane association upon tyrosine phosphorylation. In β_3MP, as in the case of β_3NP, the membrane-proximal residues (L^{717}-I^{721}) are membrane embedded and the C-terminal ^{756}NITYR^{760} motif is either membrane embedded or associated. However, unlike β_3NP, neither ^{738}KWD^{740} nor pY^{747} are inserted into or associated with the membrane (supplemental Fig. S6, *C*, *D*), which is, most probably, a direct result of tyrosine phosphorylation. The charge repulsion between the negatively charged phosphate groups of β_3MP and DPC may not allow the pY^{747} to come within close proximity to the membrane even in the presence of counterbalancing positively charged choline group. This, in turn, might affect the orientation of ^{738}KWD^{740} motif, resulting in Trp^{739} pointing in opposite direction from the membrane (Fig. 4, *C* and *F*). In β_3BP, similar to β_3NP/MP, the membrane-proximal residues (L^{717}-I^{721}) are inserted into the membrane. However, due to the phosphorylation of both tyrosines, neither the ^{738}KWD^{740}, pY^{747} nor ^{756}NITYR^{760} motifs are inserted or associated with the membrane. In summary, we have not only confirmed our earlier findings about β_3 interaction with phospholipids but also have gained some novel insights into how tyrosine phosphorylation affects these interactions and causes major conformation changes.

DISCUSSION

Many integrins share highly conserved membrane proximal helical regions (25, 26) containing GFFKR motifs in the α and HDR(R/K)E sequences in the β subunits. Earlier we have shown (7) that under aqueous conditions the membrane-proximal regions of $\alpha_{IIb}\beta_3$ integrin form a heterodimeric complex maintained by a rather famous inter-subunit clasp between residues $R^{995}(\alpha_{IIb})$ -$D^{723}(\beta_3)$ along with several other hydrophobic (α_{IIb} V^{990}-β_3 L^{718}, α_{IIb} V^{990} -β_3 I^{719}, α_{IIb} F^{992}-β_3 I^{721}) and electrostatic interactions (salt bridges between α_{IIb} R^{995}- β_3 H^{722}, α_{IIb} R^{995}- β_3 E^{726}) (Fig. 3*A*). Together these inter-subunit interactions maintain the receptor in the resting state. Recent structures of the transmembrane and cytoplasmic regions of $\alpha_{IIb}\beta_3$ heterodimer under membrane-mimetic conditions confirm this cytoplasmic clasp as an extension of coiled-coil transmembrane domains (27, 28).

Our data show that the phosphorylation of β_3 precludes this weak interaction between α and β cytoplasmic tails and, therefore, may play a critical role in maintaining the active state of the receptor during outside-in signaling. Closer examination of β_3MP structure reveals several features supporting this conclusion. The superimposition of β_3MP over β_3NP in complex with α_{IIb} (PDB ID 1M8O) shows severe steric clashes between β_3MP and the α_{IIb} subunit (Fig. 5*A*). In addition, the heterodimeric complex of integrin tails involves both hydrophobic and electrostatic interactions with Asp^{723} and Glu^{726} of β_3CT forming a salt bridge with Arg^{995} of α_{IIb}. However, in the case of β_3MP, Asp^{723} and Glu^{726} are pointing in opposite direction. Plus, in $\alpha_{IIb}\beta_3$ complex, Leu^{718} of β_3 is involved in a hydrophobic interaction with Val^{990} of α_{IIb}. In β_3MP, however, the membrane proximal hydrophobic residues interact with Trp^{739} aromatic side chain. Based on our titration experiments, we can speculate that these intramolecular interactions in β_3MP, although weak, are comparatively stronger than the weaker intermolecular interactions necessary to form $\alpha_{IIb}\beta_3$ complex. Because of several technical difficulties, we do not have structural data for the β_3BP under aqueous conditions. However, based on the similarity of phosphorylation-dependent chemical shift perturbations in the membrane-proximal region (K^{716}-D^{723}), we can propose that the β_3BP maintains a conformation similar to β_3MP. Moreover, the NMR titration experiments for β_3BP show a significant reduction in the associated chemical shift perturbations, suggesting that the bi-phosphorylation of β_3CT also favors disruption of the inter-subunit clasp. Our structural

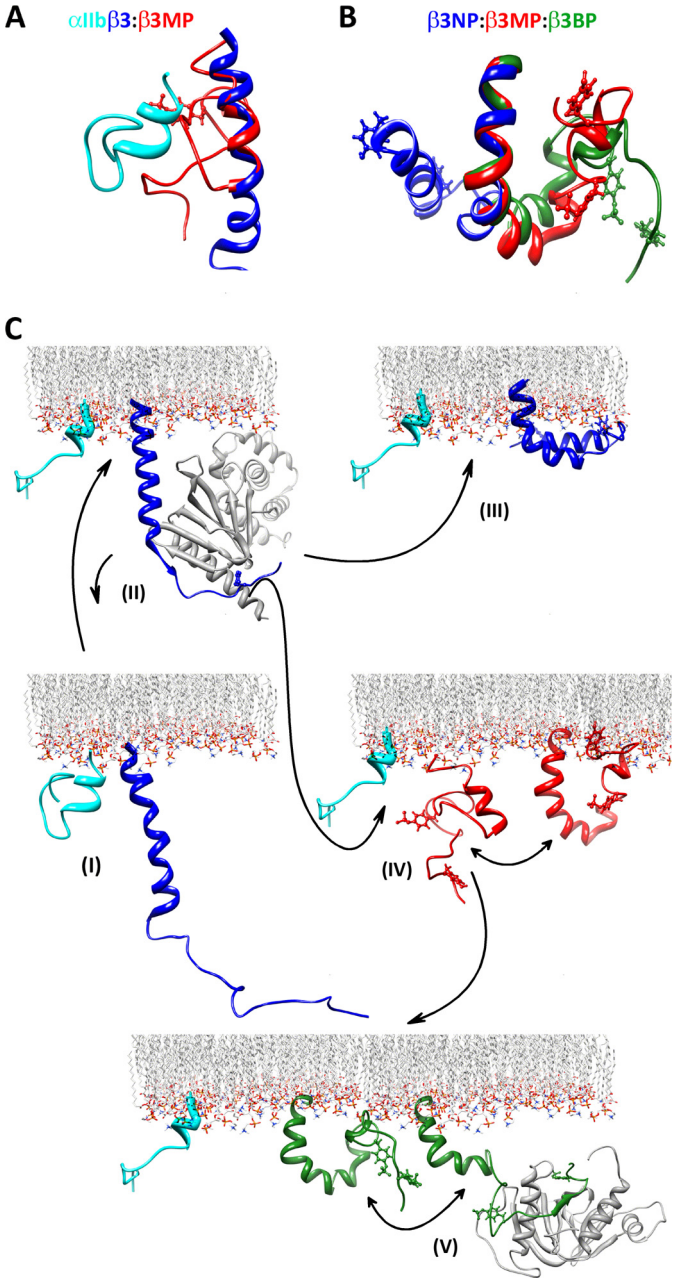

FIGURE 5. Conformational comparison between (*A*) aqueous $\alpha_{IIb}\beta_3$ heterodimer (PDB ID: 1M8O) and β_3MP; (*B*) β_3NP/MP/BP in DPC micelles. The region H^{722}-F^{727} is used for superimposition; (*C*) An equilibrium model of the integrin activation states: (*I*) resting state: $\alpha_{IIb}\beta_3$ heterodimer (PDB ID: 1M8O), the membrane proximal electrostatic and hydrophobic interactions are not shown for the sake of clarity; (*II*) activated state: upon activation, the integrin CTs separate and get inserted into the membrane. Model of activated integrin cytoplasmic tails: β_{1D}-talin2 F2F3 (PDB ID: 3G9W; (30)) and α_{IIb} in DPC micelles (PDB ID: 1S4W); (*III*) the separated tails, α_{IIb} and β_3NPin DPC micelles; (*IV*) tyrosine phosphorylation prevents the α_{IIb}-β_3 interaction; (*V*) and allows interactions with integrin-associated proteins, a model of β_3BP-Shc PTB (PDB ID: 2L1C, Ref. 31) is shown as an example. *Ribbon* representation of α_{IIb}CT is shown in cyan,β_3NP in *blue*, β_3MP in *red*, and β_3BP in *green*, whereas talin2 F2F3 and Shc PTB are shown in *gray*. The phosphorylated and non-phosphorylated tyrosines are shown with *ball and stick* while membrane is depicted in *wire* representations. Molecular graphics images were produced by using the UCSF Chimera package (29).

analysis emphasizes the role of electrostatic interaction between Lys^{738} and pY^{747} in the maintenance of the compact fold of phosphorylated β_3CT. When expressed in β_3-null endothelial cells, K738E, Y747F, and K738E/Y747F mutants diminished cell adhesion response as compared with WT integrin, thus supporting the notion that the phosphorylation-induced fold supports β_3 integrin functional activity.

In this study, we also have accumulated the first direct evidence that tyrosine phosphorylation affects the structure and the association of β_3CT with membrane. As visualized in Fig. 5*B*, charge repulsion pushes the phosphorylated tyrosine(s) away from the membrane, probably exposing alternative motifs to interact with different potential integrin-associated proteins, thus providing an additional level of complexity to the regulatory mechanisms employed in integrin signaling. A model for diversity of such interactions is presented in Fig. 5*C* based on our results. The resting state of the receptor, with the clasp between α and β subunits located within the cytosol is depicted in Fig. 5*C*, *I*. When integrin is activated, for example by talin head domain (Fig. 5*C*, *II*), α and β subunits are separated. After talin dissociation the re-clasping can be prevented and the activated state of the receptor maintained by tyrosine phosphorylation of the β subunit within cytosol (Fig. 5*C*, *IV*) as well as by membrane association of the membrane-proximal helices of a single or both subunits (Fig. 5*C*, *III*). The other functionally significant outcome of tyrosine(s) phosphorylation is the redirection of the β subunit mid-region and/or C terminus away from the phospholipid bilayer, thus allowing different adaptor proteins to bind, and, as exemplified in the case of Shc (Fig. 5*C*, *V*), propagating outside-in signaling events within cytoplasm.

To conclude, in this study, we have performed detailed NMR analysis of the effects of tyrosine(s) phosphorylation on integrin β_3CT under both aqueous and membrane-mimetic conditions. We have shown that the phosphorylation causes significant conformational rearrangement in β_3CT under solution conditions where the pY^{747} containing segment folds back and interacts with the membrane-proximal region. This arrangement prevents the β_3CT from binding to α_{IIb}CT, thus likely dictating an unclasped state of the receptor necessary to mediate integrin outside-in signaling. Moreover, tyrosine(s) phosphorylation under membrane-mimetic conditions modifies β_3CT's interaction with the membrane and perturbs its overall fold. By preventing the phosphorylated tyrosines containing regions from being inserted into or associated with the lipid bilayer phosphorylation might shift the equilibrium of integrin interactions with the different cytoplasmic adaptor proteins, adjacent receptors, and/or cytoskeleton. Our data provide a structural basis for the critical role of Tyr^{747} phosphorylation in controlling β_3CT function and shed light upon molecular details of how phosphorylation may play multiple roles in regulating different states of cell surface receptors, suggesting a more complex paradigm than a simple two state (active/inactive) model.

Acknowledgments—We thank Dr. Srikanth Rapole (UConn Mass Spectrometry Facility) for running and analyzing mass spectroscopy data. We would also like to acknowledge Liping Wu for her work on β_3CT mutants. We thank Frank Delaglio for NMRPipe, NMRDraw, and Talos+ software. We thank Dr. Alex Maltsev, Dr. Nils-Alexander Lakomek, and Dr. Yuki Takayama (NIDDK, NIH) for critical reading of this manuscript.

REFERENCES

1. Fischer, E. H., and Krebs, E. G. (1955) *J. Biol. Chem.* **216,** 121–132
2. Olsen, J. V., Blagoev, B., Gnad, F., Macek, B., Kumar, C., Mortensen, P., and Mann, M. (2006) *Cell* **127,** 635–648
3. Johnson, L. N., and Lewis, R. J. (2001) *Chem. Rev.* **101,** 2209–2242
4. Hynes, R. O. (1987) *Cell* **48,** 549–554
5. Hynes, R. O. (2002) *Cell* **110,** 673–687
6. Phillips, D. R., Prasad, K. S., Manganello, J., Bao, M., and Nannizzi-Alaimo, L. (2001) *Curr. Opin Cell Biol.* **13,** 546–554
7. Vinogradova, O., Velyvis, A., Velyviene, A., Hu, B., Haas, T., Plow, E., and Qin, J. (2002) *Cell* **110,** 587–597
8. Vinogradova, O., Vaynberg, J., Kong, X., Haas, T. A., Plow, E. F., and Qin, J. (2004) *Proc. Natl. Acad. Sci. U.S.A.* **101,** 4094–4099
9. Delaglio, F., Grzesiek, S., Vuister, G. W., Zhu, G., Pfeifer, J., and Bax, A. (1995) *J. Biomol. NMR* **6,** 277–293
10. Vranken, W., F., Boucher, W., Stevens, T., J., Fogh, R., H., Pajon, A., Llinas, M., Ulrich, E., L., Markley, J., L., Ionides, J., and Laue, E., D. (2005) *Proteins*, 687–696
11. Wuthrich, K. (1986) *NMR of Proteins and Nucleic Acids*, John Wiley & Sons, New York
12. Shen, Y., Delaglio, F., Cornilescu, G., and Bax, A. (2009) *J. Biomol. NMR* **44,** 213–223
13. Güuntert, P. (2004) *Methods Mol. Biol.* **278,** 353–378
14. Linge, J. P., Williams, M. A., Spronk, C. A., Bonvin, A. M., and Nilges, M. (2003) *Proteins* **50,** 496–506
15. Brunger, A. T., Adams, P. D., Clore, G. M., DeLano, W. L., Gros, P., Grosse-Kunstleve, R. W., Jiang, J. S., Kuszewski, J., Nilges, M., Pannu, N. S., Read, R. J., Rice, L. M., Simonson, T., and Warren, G. L. (1998) *Acta Crystallogr. D. Biol. Crystallogr.* **54,** 905–921
16. Anthis, N. J., Haling, J. R., Oxley, C. L., Memo, M., Wegener, K. L., Lim, C. J., Ginsberg, M. H., and Campbell, I. D. (2009) *J. Biol. Chem.* **284,** 36700–36710
17. Ulmer, T. S., Yaspan, B., Ginsberg, M. H., and Campbell, I. D. (2001) *Biochemistry* **40,** 7498–7508
18. Clore, G. M., and Gronenborn, A. M. (1982) *J. Magn. Reson.* **48,** 402–417
19. Qin, J., Vinogradova, O., and Gronenborn, A. M. (2001) *Methods Enzymol.* **339,** 377–389
20. Deshmukh, L., Tyukhtenko, S., Liu, J., Fox, J. E., Qin, J., and Vinogradova, O. (2007) *J. Biol. Chem.* **282,** 32349–32356
21. Metcalf, D. G., Moore, D. T., Wu, Y., Kielec, J. M., Molnar, K., Valentine, K. G., Wand, A. J., Bennett, J. S., and DeGrado, W. F. (2010) *Proc. Natl. Acad. Sci. U.S.A.* **107,** 22481–22486
22. Li, R., Babu, C. R., Valentine, K., Lear, J. D., Wand, A. J., Bennett, J. S., and DeGrado, W. F. (2002) *Biochemistry* **41,** 15618–15624
23. Kosen, P. A. (1989) *Methods Enzymol.* **177,** 86–121
24. Hilty, C., Wider, G., Fernández, C., and Wüthrich, K. (2004) *Chembiochem* **5,** 467–473
25. Vinogradova, O., Haas, T., Plow, E. F., and Qin, J. (2000) *Proc. Natl. Acad. Sci. U.S.A.* **97,** 1450–1455
26. Li, R., Babu, C. R., Lear, J. D., Wand, A. J., Bennett, J. S., and DeGrado, W. F. (2001) *Proc. Natl. Acad. Sci. U.S.A.* **98,** 12462–12467
27. Yang, J., Ma, Y. Q., Page, R. C., Misra, S., Plow, E. F., and Qin, J. (2009) *Proc. Natl. Acad. Sci. U.S.A.* **106,** 17729–17734
28. Lau, T. L., Kim, C., Ginsberg, M. H., and Ulmer, T. S. (2009) *EMBO J.* **28,** 1351–1361
29. Pettersen, E. F., Goddard, T. D., Huang, C. C., Couch, G. S., Greenblatt, D. M., Meng, E. C., and Ferrin, T. E. (2004) *J. Comput. Chem.* **25,** 1605–1612
30. Anthis, N. J., Wegener, K. L., Ye, F., Kim, C., Goult, B. T., Lowe, E. D., Vakonakis, I., Bate, N., Critchley, D. R., Ginsberg, M. H., and Campbell, I. D. (2009) *EMBO J.* **28,** 3623–3632
31. Deshmukh, L., Gorbatyuk, V., and Vinogradova, O. (2010) *J. Biol. Chem.* **285,** 34875–34884
32. Dosset, P., Hus, J.-C., Blackledge, M., and Marion, D. (2000) *J. Biomol. NMR* **16,** 23–28